Earth and Planetary Science Letters 450 (2016) 62–70

Contents lists available at ScienceDirect

Earth and Planetary Science Letters

www.elsevier.com/locate/epsl

Seismic imaging of a mid-lithospheric discontinuity beneath Ontong Java Plateau

Saikiran Tharimena *, Catherine A. Rychert, Nicholas Harmon

Ocean and Earth Science, University of Southampton, United Kingdom

ARTICLE INFO

Article history:
Received 21 January 2016
Received in revised form 10 June 2016
Accepted 17 June 2016
Available online 30 June 2016
Editor: J. Brodholt

Keywords:
mid-lithospheric discontinuity
Ontong Java Plateau
anomalous lithosphere
SS precursors
viscous root

ABSTRACT

Ontong Java Plateau (OJP) is a huge, completely submerged volcanic edifice that is hypothesized to have formed during large plume melting events ~90 and 120 My ago. It is currently resisting subduction into the North Solomon trench. The size and buoyancy of the plateau along with its history of plume melting and current interaction with a subduction zone are all similar to the characteristics and hypothesized mechanisms of continent formation. However, the plateau is remote, and enigmatic, and its proto-continent potential is debated. We use SS precursors to image seismic discontinuity structure beneath Ontong Java Plateau. We image a velocity increase with depth at 28 ± 4 km consistent with the Moho. In addition, we image velocity decreases at 80 ± 5 km and 282 ± 7 km depth. Discontinuities at 60–100 km depth are frequently observed both beneath the oceans and the continents. However, the discontinuity at 282 km is anomalous in comparison to surrounding oceanic regions; in the context of previous results it may suggest a thick viscous root beneath OJP. If such a root exists, then the discontinuity at 80 km bears some similarity to the mid-lithospheric discontinuities (MLDs) observed beneath continents. One possibility is that plume melting events, similar to that which formed OJP, may cause discontinuities in the MLD depth range. Plume–plate interaction could be a mechanism for MLD formation in some continents in the Archean prior to the onset of subduction.

1. Introduction

Several hypotheses have been put forward to explain continent formation. It has been suggested that cratons were formed by large mantle plume-related melting events that led to compositional depletion (Boyd, 1989), stacking of young ocean lithosphere (Calvert et al., 1995), or island arc accretion with orogenic thickening at subduction zones (Lee et al., 2011; Taylor and Mclennan, 1995), although no consensus has been reached (Lee et al., 2011). New constraints on the structure of continental cratons from seismic imaging techniques offer promising insights to the original formation mechanism of the cratons. For instance, discontinuities have recently been imaged in the 60–110 km depth range beneath the continents (Rychert and Shearer, 2009; Rychert et al., 2010; Selway et al., 2015), termed mid-lithospheric discontinuities (MLD). These features are enigmatic in that the physical and chemical properties that define them are not well-understood. Observations of strong sharp seismic velocity gradients suggest mechanisms besides temperature, such as melt or hydration are required (Rychert et al., 2005), although continental cratons are not likely stable in the presence of water or melt at the quantities required by seismic data (Faul, 1997; Hirth and Kohlstedt, 1995, 1996). Furthermore, although MLDs are likely related to the formation and/or the evolution of the continents, the exact connection has not been established. For instance, they may represent relict stacked slab structures (Bostock, 1999), metasomatic fronts (Selway et al., 2015; Tommasi and Ishikawa, 2014), elastically accommodated grain boundary sliding (Karato et al., 2015), or frozen-in compositional interfaces, possibly related to a previous plume melting event.

Here we focus on the seismic velocity structure of Ontong Java Plateau (OJP), a huge, completely submerged, ~120 My old volcanic edifice, more than half the size of Australia that likely formed by plume volcanism (Coffin and Eldholm, 1994). Its surface area (including Nauru, eastern Mariana and Pigafetta basins), 4.11×10^6 km^2, covers 0.8% of the Earth (Coffin and Eldholm, 1994) and may be part of a much larger super-plateau that also included Manihiki and Hikurangi plateaus (Chandler et al., 2013). The separation of the plateaus likely occurred via interaction with a nearby triple junction around the time of formation (isochrons in Fig. 1). OJP now lies at the junction between

* Corresponding author at: National Oceanography Centre, University of Southampton, Waterfront Campus, European Way, Southampton SO14 3ZH, United Kingdom.
E-mail address: S.Tharimena@noc.soton.ac.uk (S. Tharimena).

http://dx.doi.org/10.1016/j.epsl.2016.06.026

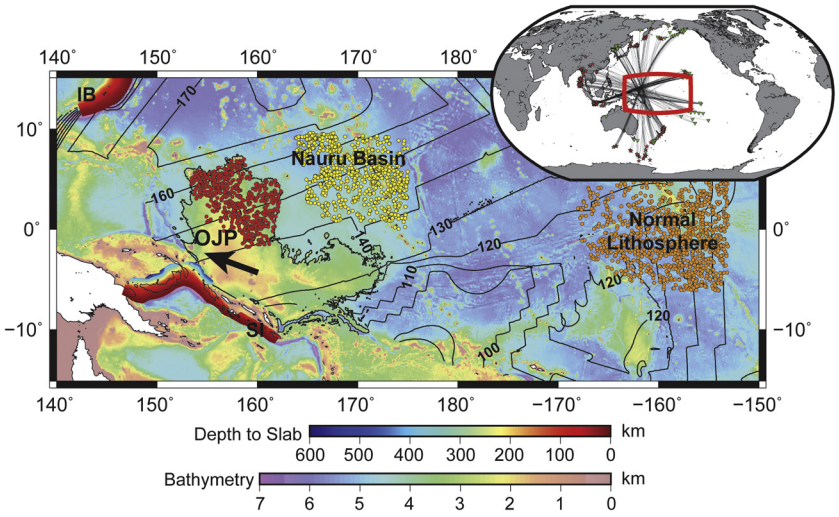

Fig. 1. Bathymetry map of the western Pacific with Ontong – Java Plateau (OJP) marked by 4000 m isobath. Colored circles show bouncepoints beneath OJP (red), Nauru basin (yellow) and normal oceanic lithosphere (orange) (Korenaga and Korenaga, 2008). Colored overlays labeled SI and IB show subducted slabs (Hayes et al., 2012) along the Solomon Islands (SI) and the Izu–Bonin–Mariana trench (IB). Background colors show bathymetry and contours represent the age of seafloor in My (Muller et al., 2013). Black arrow shows the present plate motion direction. Overlay global map shows the study region (red box) and event (red star)–station (green inverted triangle) pairs that have bouncepoints beneath OJP.

the Pacific and Australian plates due to collision along the southern and southwestern boundaries with the Solomon Islands arc (Mann and Taira, 2004). OJP shares common elements to all of the suggested models of continent formation described above, i.e. it was formed by a large melting event which generated buoyancy – it is now resisting subduction (Mann and Taira, 2004; Miura et al., 2004), and it may eventually cause slabs to stack and/or terranes to be accreted to form a new continent. OJP's remarkable stability, low subsidence (Ito and Clift, 1998) and resistance to subduction supports comparisons to continents, leading some to suggest it represents a modern-day proto-craton (Lee et al., 2011), and an ideal place to test hypotheses for the formation of continents.

Seismic refraction and gravity studies have constrained the thick crustal structure of the OJP, an average crustal thickness of 32 km (Furumoto et al., 1976; Mann and Taira, 2004; Miura et al., 2004) and a high velocity lower crust, characteristic of large igneous provinces (Coffin and Eldholm, 1994). It has been suggested that the lower crust beneath OJP is composed of granulite facies that formed due to recrystallization of ponded and fractionated picritic melts that were emplaced during a plume event in an oceanic, plate boundary setting (Gladczenko et al., 1997; Miura et al., 2004). The free air gravity anomaly of the plateau suggests that OJP is isostatically compensated (Gladczenko et al., 1997). However, in addition to the crust, a mantle component is thought to be required to support its topography (Gladczenko et al., 1997; Ito and Taira, 2000). Previous constraints on OJP mantle structure suggest that it is different than surrounding regions. Analysis of multiple-ScS waves suggests low shear attenuation ($QScS = 253–366$) beneath OJP in comparison to surrounding regions (Gomer and Okal, 2003), which was interpreted as a viscous mantle lithospheric root (Klosko et al., 2001). Similarly, variations in shear wave splitting measurements on and off the plateau suggest that asthenospheric flow is perturbed around a root-like structure that is chemically distinct and rheologically strong (Klosko et al., 2001). Regional surface wave tomography similarly suggests an anomalous mantle lithosphere beneath OJP (Covellone et al., 2015; Richardson et al., 2000). Richardson et al. (2000) found shear velocities 5% slower than surrounding regions, i.e., the opposite sense of typical expectations for a viscous, rigid root. Although Covellone et al. (2015) suggests fast shear velocities on an average across the whole plateau, the mantle lithosphere beneath northern OJP, the focus of this study, is relatively slow compared to surrounding regions (Covellone et al., 2015; French et al., 2013). These seemingly contradictory and intriguing results add to the enigma of the remote, yet massive plateau region, where in-situ measurements are scarce and seismic imaging has proven challenging.

Here we use SS precursors to image velocity discontinuities beneath the remote OJP. SS precursors are powerful in that they have sensitivity in locations where station coverage is sparse (Rychert and Shearer, 2011).

2. Methods

We use SS precursors method of Rychert and Shearer (2010, 2011) to image lithospheric structure beneath the plateau. SS precursors are underside reflections from velocity discontinuities that arrive before the main SS phase due to shorter paths through the upper mantle (Rychert and Shearer, 2011). SS precursors are sensitive to the discontinuity structure near the bouncepoint, which is halfway between the source and the receiver. We focus on imaging the northern part of OJP to avoid complications from subduction zone structures on the southern margin of the plateau (Fig. 1).

2.1. Stacking

We used the Incorporated Research Institutions for Seismology (IRIS) earthquake dataset from 1990 to 2009 with event to station (epicentral) distances of 90° to 140°. The waveforms are pre-processed to remove instrument response. We use events with magnitude >5.5 Mw and restrict source depth to <75 km depth to minimize complications arising from depth phases (Rychert and Shearer, 2011). The horizontal components are rotated to radial and transverse components. We consider the transverse components, Hilbert transforming them to produce symmetric pulses. The waveforms are then low-pass filtered at 0.1 Hz. We then align the waveforms, centered on the maximum amplitude (positive or negative), in a window 40 s before and after the theoretical SS arrival time. The centered waveforms are normalized and the polarity of negative pulses flipped to align with the maximum positive pulse. Signal-to-noise ratio (SNR) of each waveform is calculated using standard deviation in a window 250 s to 25 s before the SS peak and, we reject waveforms with SNR less than four. Waveforms with long period noise were also rejected by discarding those

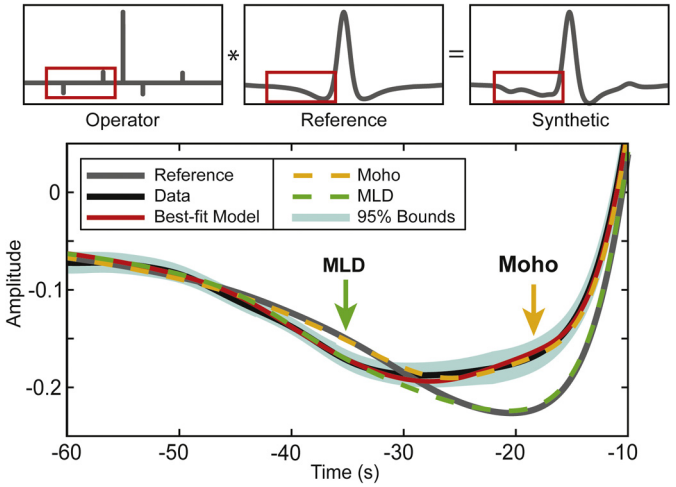

Fig. 2. Schematic of a lithospheric operator (e.g. Moho and mid-lithospheric discontinuity) convolved with a reference waveform to generate a synthetic model (top). Bottom panel shows models with only a Moho (orange), only mid-lithospheric discontinuity (green), and best-fitting model that requires both Moho and mid-lithospheric discontinuity (red). Solid black line shows SS stack beneath OJP and solid grey line is the reference waveform. Error surface is represented by 95% confidence bounds.

waveforms whose SS precursor side lobe has a zero crossing of >20 s. We obtain 3450 waveforms that fit the source parameters described above, 540 of which also fit the SNR criteria. The waveforms are weighted according to their SNR before stacking and the final stack is normalized to unit amplitude.

2.2. Discontinuity modeling

Owing to the long period of the SS precursors (10–20 s), the underside reflections from the crust and the lithosphere do not appear as a distinct phase, but they affect the character of the SS stack (Rychert and Shearer, 2010). This variation in the character of SS stack is exploited to constrain the depth and velocity structure of the plateau using velocity discontinuity operators.

We model discontinuity structure beneath the plateau using the method of Rychert and Shearer (2011). Synthetic waveforms were produced by convolving velocity discontinuity operators with a reference waveform (Fig. 2). A Grid-search was used to determine the best-fitting model with the lowest sum of absolute residuals. We used an F-test to determine statistical significance of the model parameters. The number of degrees of freedom in the data waveform was determined using autocorrelation of SS waveform. We estimated 11 degrees of freedom in the data in the time window used in the inversions. Our final result resolves 7 total model parameters, 3 for each of the 2 deeper negative discontinuities (amplitude, depth, and Gaussian width) and 1 for the Moho (depth). We model only SS precursors i.e. the time series preceding the SS phase. We allow both positive (velocity increase with depth such as at Moho) and negative (velocity decrease with depth such as the lithosphere–asthenosphere boundary) discontinuities in our models. We use a Gaussian function to investigate a range of discontinuity sharpnesses, i.e., step functions to gradual velocity changes (Rychert and Shearer, 2011). The sharpness of discontinuities reported in the text represents four times the Gaussian half-width, or $\pm 2\sigma$. The model that yields the best-fit synthetic and is statistically significant is inverted to determine the depth, sharpness and amplitude of velocity discontinuities.

The 1-D shear velocity–depth profile is calculated from our constraints on seismic discontinuities. Operator amplitudes are scaled to velocity variation using the equation for SS reflection coefficients (Aki and Richards, 2009). We assume densities from PREM (Dziewonski and Anderson, 1981) noting that SS is affected by both density and velocity, and we do not have the ability to distinguish between the two. We construct the 1-D profile starting at the base of the root where we assume PREM velocity at 300 km depth, implementing the constrained velocity variations one by one, moving towards the surface of the Earth. Similarly, depth is scaled from the delay time of the operator, assuming the velocities of the profile. Depth is a function of the two-way travel time between the discontinuity and the free surface. The depth of discontinuity, assuming a plane wave approximation, is given by:

$$h = \sum_{0}^{i} \frac{\partial \tau_i}{2\sqrt{\beta_i^{-2} - p^2}} \tag{1}$$

where h is the depth, $\partial\tau$ is the delay time, β is the shear velocity, and subscript i is the step interval. We assume an average horizontal slowness, $p = 0.12\ \mathrm{s\,km^{-1}}$. We also include a gradual, linear velocity gradient between 80–280 km for consistency with other work (French et al., 2013; Richardson et al., 2000), although our waveforms do not provide constraints on such gradual features.

The reference waveform is generated using a similar procedure to that of OJP stack. We used 55,200 waveforms that have SS bouncepoints beneath the Pacific to generate the reference stack. We exclude waveforms that have bouncepoints beneath the region 10° around the OJP to avoid contamination of the reference waveform.

In our modeling procedure, we systematically increased the number of operators to determine the number of statistically significant discontinuities required to explain the observations. We used an F-test for significance of regression to establish the significance of additional discontinuities. The polarity of discontinuities was also allowed to vary (positive or negative) to test for the bias in depth estimates due to contamination from sidelobes of nearby discontinuities. Error estimation for model parameters is based on bootstrap resampling with replacement and grid-search estimation. For bootstrap resampling we stack the same number of SS waveforms in the original data stack, randomly resampling waveforms included in the original stack allowing repetition of waveforms. We perform 100 bootstraps and use an automated grid search procedure to determine the best-fitting model parameters for each bootstrap. The error in the model parameters corresponds to the range of model parameters within the bootstrapped limits of the data. An F-test was also performed on the bootstraps to validate the significance of the discontinuities. The error is determined by 95% confidence limits, which corresponds to two standard deviations of the mean of the resulting variability in the bootstraps. We test for the simplest yet robust model that fits the data and explains the observations.

We investigated the effects of data filtering on sidelobes and our final results. However, there is no discernable difference in the waveform when frequencies above the low-pass used here (0.1 Hz) are included, well within the error bounds on the data. We do not apply a high-pass filter to the data in our processing. Our discontinuity results are robustly resolved. Indeed, the method used here has been shown to accurately recover Moho depths across Asia, as evidenced by high correlation with CRUST2.0, as determined by independent constraints (Rychert and Shearer, 2010).

2.3. Thermal modeling

Since OJP is suggested to have formed due to a massive melting event, we tested how long a thermal anomaly could persist after an initial plume head arrival using a 2-D numerical model of mantle convection. We model mantle flow, mantle temperature, melting and depletion in a 2D vertical cross section approximating

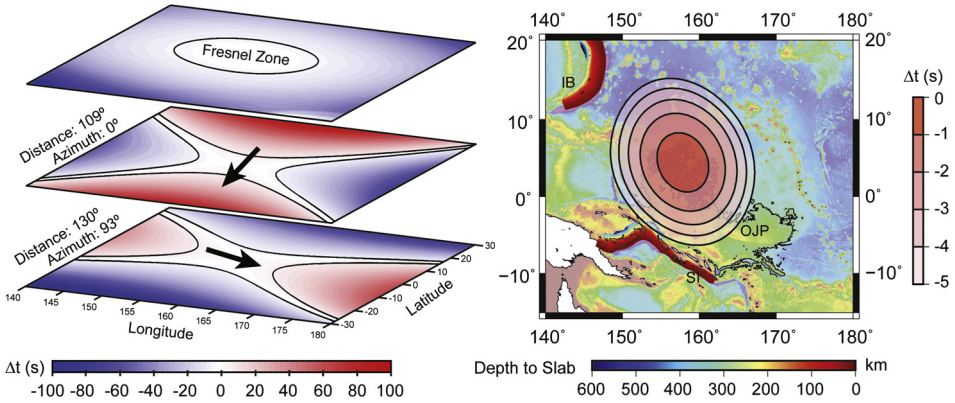

Fig. 3. Fresnel zone for SS reflected off of a discontinuity at 282 km depth. Panel on left shows contour of travel time difference for lateral perturbations to the SS bouncepoint. The Fresnel zone is defined by a $\pm T/4$ contour. The top panel shows the effective Fresnel zone which is computed by summation of travel time differences for different event–station offsets. Arrows indicate the direction of propagation of the wave from event to receiver. Contours on the map show sensitivity of the Fresnel zone at intervals of 1 s. The sensitivity of Fresnel zone reduces from the center, indicated by the dark red hue, towards the periphery. Colored overlays show the SI and IB slabs (Fig. 1).

the Ontong Java Plateau using the method of Jha et al. (1994), and Harmon and Blackman (2010). This method uses a finite element solver for mantle flow and a finite difference scheme for the heat equation (Jha et al., 1994; Smolarkiewicz, 1984). In the model we allow mantle melting due to the excess temperature and depletion, using the melting model of Katz et al. (2003). We allow thermally driven convection in addition to melt and depletion buoyancy effects.

The mesh of our finite element model was made up of irregularly sized rectangular elements with 201×71 nodes, representing a 2000 km wide by 700 km deep box (Supplementary Fig. S1). The sides and bottom of the model are stress free, allowing inflow and outflow as necessary to accommodate the plate kinematics. We assign a zero plate velocity along the top boundary to simulate ridge perpendicular motion in 2D. Thermal boundary conditions are fixed temperatures at the top of the model of 0 °C and a specified mantle potential temperature, T_m of 1350 °C plus a mantle adiabat at the bottom of 0.3 °C/km. In our numerical experiment viscosity is pressure and temperature dependent assuming an Arrhenius form of viscosity after (Conder et al., 2002; Harmon and Blackman, 2010) that produces viscosities within the ranges for a linearized dislocation creep (Conder et al., 2002) and diffusion creep (Hirth and Kohlstedt, 1996; Karato and Wu, 1993). We limit the maximum value of viscosity to 10^{23} Pa s in the lithosphere for potential temperatures <700 °C. For our initial condition, we start with a background thermal structure for a 30 My plate, and superimpose a 200 °C thermal anomaly between 50–300 km depth and −500 to 500 km from the center. We allow the model to evolve through time for 92 My.

2.4. Fresnel zone testing

We investigated the possibility of off-axis slab structures manifesting in our OJP data at the deepest interface considered here, 282 km depth. We calculated the Fresnel zone for each bouncepoint by plotting travel time differences for non-specular reflection points from the specular reflection or the midpoint along the great circle path. The Fresnel zone for each individual bouncepoint corresponds to the saddle shaped region for which the travel time difference is $<\pm T/4$, where T is the dominant period, ∼20 s for SS (Fig. 3). We stacked the Fresnel zones of our SS data finding a ∼10° disc centered on the northern OJP (Fig. 3). Our event–station distribution limits the effects of off-axis structure including the subducting slab along Solomon Islands, which is outside the region of sensitivity.

2.5. Moveout testing

We also investigated the effect of moveout on our final result, i.e. variation in precursor-SS differential travel times for different event–station distances, which is greater for deeper discontinuity depths. We focus on the deepest interpreted phase at 282 km. Our stacks are dominated by waveforms arriving from an epicentral distance of 90°–120°, and stacks including only those smaller distances are nearly identical to those that include the larger distance range. The moveout for an arrival from ∼282 km depth within this range is ∼4 s (Supplementary Fig. S2). This is less than 1/4 of the dominant wave period (20 s) used in our study. Further, the stack with waveforms arriving from 90°–120°, where there is less effect of moveout, is slightly broader, i.e. the opposite of expectation from moveout (Supplementary Fig. S2). This suggests that we are not detecting a difference caused by moveout. Therefore, while moveout may affect our constraints on the sharpness of the phase at 282 km, making the discontinuity appear slightly more gradual; it would not significantly affect our ability to image the discontinuity of interest. In practice the effect of moveout is incorporated within the error limits from the bootstrap.

3. Results

The OJP waveform at 0 to −45 s is characterized by a broad lower amplitude sidelobe in comparison to other oceanic waveforms (Fig. 4). This is likely owing to the thickened OJP Moho, as corroborated by the inversion results and discussed below. In addition, a significant pulse appears in the OJP stack near 282 km, which is not present in any other 10° oceanic bins.

Waveform modeling the OJP stack suggests three distinct, significant discontinuities beneath the plateau (Fig. 4). We find a velocity increase (positive polarity) at 28 ± 4 km consistent with the Moho. A velocity decrease of $6 \pm 4\%$ is imaged at a depth of 80 ± 5 km and a velocity decrease of $5 \pm 4\%$ at a depth of 282 ± 7 km, were also imaged (Figs. 4a, 5a). The negative discontinuities imaged at ∼80 km and ∼282 km are sharp, occurring over <17 km depth. We present a best-fitting 1-D model that incorporates these seismic velocity discontinuities. The model assumes PREM velocity at 300 km depth since our results only constrain changes in velocity, rather than absolute velocity.

Finally, our numerical modeling test for the longevity of a thermal anomaly suggests that the majority of the thermal anomaly is dissipated within the first 30 My and the anomaly is entirely dissipated after 50 My. Supplementary Fig. S1a and S1b shows the initial thermal structure and the thermal structure at 47 My, with

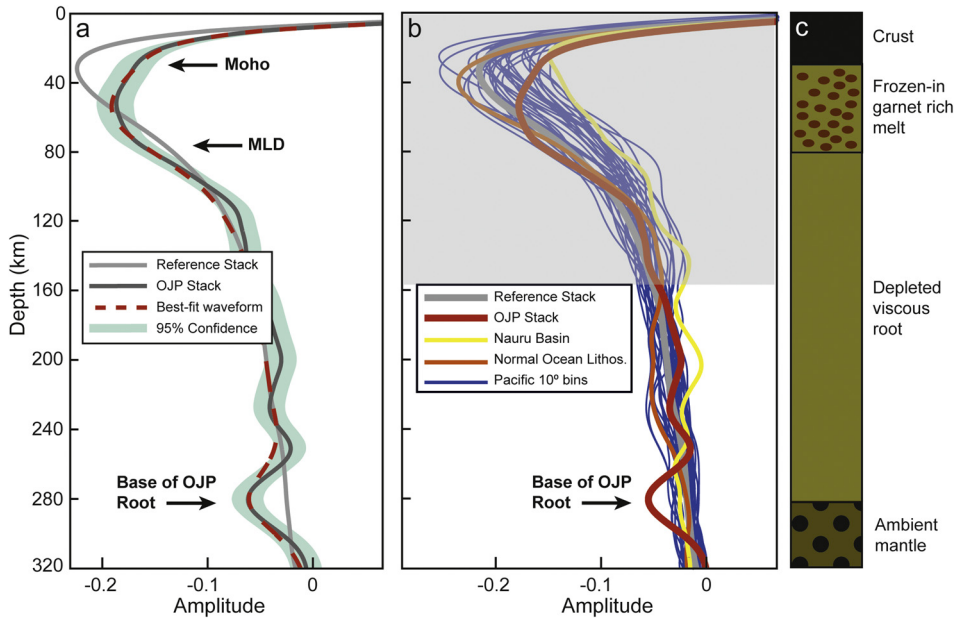

Fig. 4. Waveform fit and discontinuity structure beneath OJP. (a) Best-fit model (red dashed) compared to the OJP data (dark grey) and reference waveform (grey). Green shaded area shows 95% confidence limits. (b) OJP data stack compared to SS stacks beneath Nauru basin (yellow), normal oceanic lithosphere (orange), and 10° bouncepoint bins in the Pacific with >500 waveforms (blue). The shallow part of waveforms in the center panel has been greyed out to highlight the deeper discontinuity at 282 km which is not observed elsewhere in the Pacific. (c) Interpretive schematic of the root structure beneath OJP.

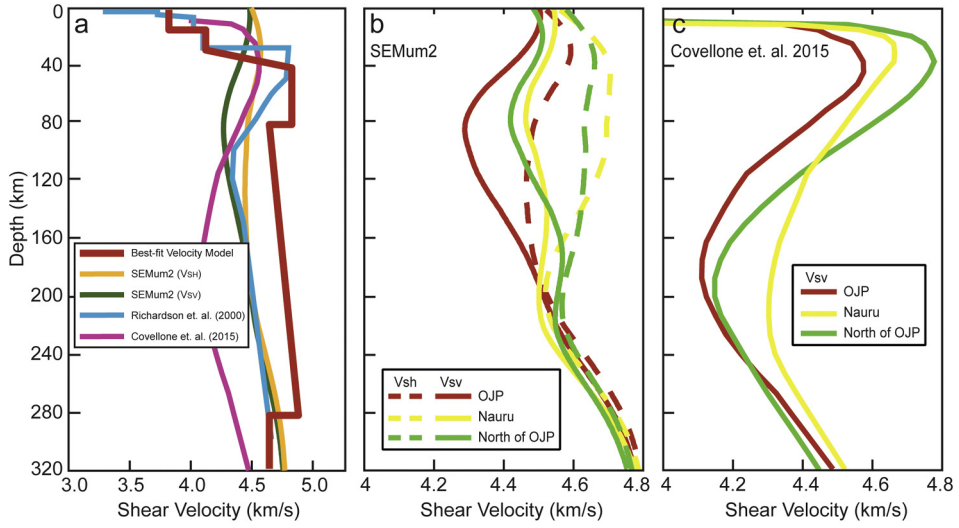

Fig. 5. Discontinuity structure and velocity model beneath OJP compared to surface wave studies. (a) Velocity models beneath the study area on northern OJP. Surface wave velocity models beneath northern OJP (red), Nauru (yellow) and the Pacific ocean north of OJP (green) from (b) SEMum2 (French et al., 2013) and (c) Covellone et al. (2015).

the thermal structure at the center of the original thermal anomaly plotted in Supplementary Fig. S1c. At 47 My, the thermal anomaly is $<10\,^{\circ}$C than the expected value from a half-space cooling model. The persistence of the anomalous structure today, 90 My after the last volcanic rejuvenation event, suggests a mechanism other than a purely thermal origin.

4. Discussion

The 28 ± 4 km deep Moho is in agreement with previous refraction work that found an average crustal thickness of 32 km (Furumoto et al., 1976; Miura et al., 2004). The fact that SS also requires such a deep Moho, in comparison to typical oceanic Moho depths, suggests that the thickened crust extends over a wide lateral area of the plateau. This is consistent with surface wave Moho estimates in the northern plateau area, which ranges from 26–32 km (Richardson et al., 2000).

The discontinuity at 80 km coincides with the gradual decrease in surface wave SV velocities from ~40 to 120 km depth (Covellone et al., 2015; French et al., 2013; Richardson et al., 2000). Velocity decreases with depth have been frequently imaged across at least some large sections of the Pacific in the 60–80 km depth range (Gaherty et al., 1999; Rychert and Shearer, 2011; Schmerr, 2012; Tan and Helmberger, 2007) including beneath the Hikurangi plateau (Stern et al., 2015), which is thought to have once been part of the same super plateau as OJP (Chandler et al., 2013). Our 80 km discontinuity may be related to other oceanic results and/or other results from ocean plateaus. Alternatively, our observation could also be different than those of normal ocean lithosphere owing to the large melting event that is hypothesized to have formed the plateau. The same is true for OJP's sister plateaus which have had divergent histories for the past ~120 My.

The discontinuity at 282 km is the opposite sense (a velocity decrease with depth) in comparison to surface wave results that

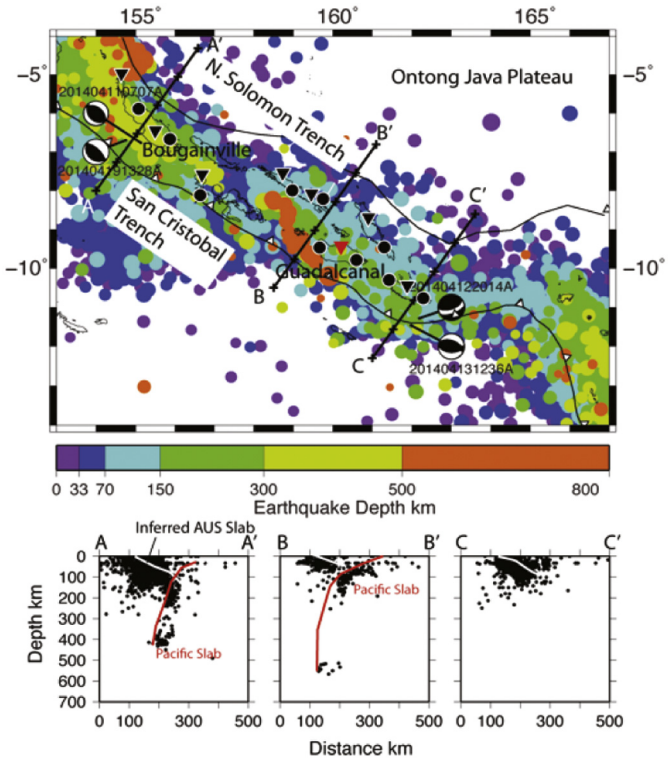

Fig. 6. Map of seismicity from 1964–2014 color coded by depth (top). Focal mechanisms of April 2014 major earthquakes shown. Bottom panels show profiles of earthquakes depth within 100 km of profile line (A–A′, B–B′, C–C′ indicated on map, *x*'s indicate 100 km ticks). Interpreted slab interfaces drawn on for reference (White = Australian, Red = Pacific). Red triangle is GSN station HNR.

find slow velocities down to 250–300 km depth in comparison to surrounding regions and deeper depths (Covellone et al., 2015; Richardson et al., 2000). A gradual increase in velocity with depth from 80 to 282 km depth could reconcile the surface waves with the SS constraints (Fig. 5a). The 282 km depth discontinuity beneath OJP is also unique. Although some observations of discontinuities at 250–330 km depth have been reported, referred to as Lehmann or X, they are opposite in sign (+) in comparison to our (−) observations, more frequently associated with subduction, only rarely beneath the oceans (Bagley and Revenaugh, 2008; Deuss and Woodhouse, 2002). We do not see evidence for these positive phases in our 10° bins. We emphasize that although the region borders a subduction zone, our Fresnel zone is well outside the slab (Fig. 3) as predicted by local tectonic, tomography, and earthquake locations (Fig. 6). In addition, other bins of ours just as close to subduction show no sign of such a signature. Indeed, the OJP waveform looks very different at time differentials corresponding to 282 km depth from all other 10° bouncepoint bins of the Pacific, surrounding lithosphere in the Nauru Basin, or nearby "normal" lithosphere (Korenaga and Korenaga, 2008), closest in age (100–150 My) to that underlying OJP (130–150 My) (Fig. 4b). This suggests that the OJP may be different from normal oceanic mantle down to great depth, ∼282 km. An anomalous OJP mantle to ∼282 km depth is evidenced in other studies as well. OJP is characterized by lower attenuation than surrounding regions (Gomer and Okal, 2003). It also appears seismically slower in global models (French et al., 2013) and regional surface wave models (Covellone et al., 2015; Richardson et al., 2000) (Fig. 5).

The physical processes that produce the 80 km and 282 km discontinuities may yield insights into the formation mechanism of the OJP. Mechanisms such as changes in anisotropy (Beghein et al., 2014; Kawakatsu et al., 2009; Rychert et al., 2014), hydration (Karato et al., 2015), melt (Hirschmann, 2010; Kawakatsu et al., 2009), or composition (Gaherty et al., 1999) may explain apparent velocity decreases with depth beneath the oceans.

4.1. Anisotropy

Anisotropic variations could explain apparent velocity discontinuities in SS waveforms (Rychert et al., 2014). Variability in our northern OJP study region is difficult to decipher from the broad scale of global models (Beghein et al., 2014; Maggi et al., 2006). However, azimuthal anisotropy is generally weak compared to surrounding regions in the 50–400 km depth range near OJP (Maggi et al., 2006). Many of our waveforms travel in a W–E or E–W direction. Therefore, if large azimuthal anisotropy did exist beneath northern OJP it could explain an apparent velocity decrease with depth if the fast direction were oriented N–S above or W–E below either the 80 km or the 282 km discontinuities. However, such orientations would not necessarily explain the anomalous nature of the mantle down to 282 km depth in comparison to surrounding regions as observed by other studies. For instance, a W–E orientation from 80–282 km could explain slow N–S traveling Rayleigh wave velocities (Richardson et al., 2000), although not the ∼282 km discontinuity in our result or low attenuation in the region (Gomer and Okal, 2003). Overall, another mechanism would be required to explain why the region is anisotropically anomalous in comparison to surrounding regions (Klosko et al., 2001; Tommasi and Ishikawa, 2014). An increase in radial anisotropy (SH > SV) with depth can produce an apparent velocity decrease with depth in SS precursors. The anisotropy could be produced by layering or random distribution of olivine a-axes in the horizontal plane. However, surface wave models suggest decreasing radial anisotropy with depth from 80 to >282 km under northern OJP (Fig. 5b) (Covellone et al., 2015; French et al., 2013). In addition, as for the azimuthal anisotropy case, some other mechanism would still also be required in combination with the anisotropy either from very special current day tectonics or as a frozen-in signature to make the area distinct to 282 km in comparison to surrounding regions. Therefore, while we cannot preclude anisotropic effects, a purely anisotropic explanation for the OJP mantle is not consistent with seismic models, in which the plateau is isotropically anomalous in comparison to surrounding regions to depths of 200–300 km (Covellone et al., 2015; French et al., 2013; Richardson et al., 2000). Some other cause is also likely required to explain the anomalous OJP mantle.

4.2. Active tectonics

The best-fitting 80 km discontinuity is sharp, occurring over <17 km and an increase in hydration or melt with depth could explain such a sharp discontinuity. Increased water or melt at >80 km would weaken the mantle, and likely represent the LAB, precluding the possibility of a deeper viscous root beneath 80 km. Without a viscous root (e.g. hydration or melt between 80–282 km depth), an alternative explanation of anomalous mantle structures at deeper depths in surface wave velocity (Covellone et al., 2015; Richardson et al., 2000), attenuation (Gomer and Okal, 2003), the 80 km discontinuity and also the anomalous discontinuity at 282 km of this study would be required. However, there is no evidence for a simple active tectonic explanation for the discontinuities at 80 km or 282 km depth. Subduction tectonics at the North Solomon Trench are several 100s of kilometers south of our study area, with no evidence of slab transport towards our study region in the north in surface wave tomography (Covellone et al., 2015). Indeed, slab descent is steeply dipping and focused beneath the Solomon and New Guinea Islands, down to ∼600 km depth (Fig. 6), as illuminated by earthquake locations (Cooper and Taylor, 1985). In addition, there is no evidence for slab stagnation above

the 410 km discontinuity in global surface wave studies (French et al., 2013) and P wave tomographic model (Fukao and Obayashi, 2013). Finally, xenoliths from the margins are consistent with a stable root structure related to anomalous mantle melting that extends to at least 120 km, i.e., deeper than the 80 km discontinuity (Tommasi and Ishikawa, 2014), implying that the 80 km discontinuity may not be the LAB. The xenoliths are from the plateau margin, 100s of km away from the center of our study region, where the plateau may be thinner, and likely reflect a minimum thickness for the plateau.

4.3. Elastically accommodated grain boundary sliding (EAGBS)

The 80 km discontinuity occurs at a similar depth and with similar gradient parameters as those observed across the Pacific (Rychert and Shearer, 2011; Schmerr, 2012). One possibility is that it is related to EAGBS, in which the effect of water on seismic waves is enhanced without necessarily causing a strong variation in viscosity (Karato et al., 2015). Although, the importance of this effect is debated (Jackson and Faul, 2010) and experimental work on hydration is beginning to emerge (Aizawa et al., 2008).

4.4. Compositional origin, possibly in a viscous root

Our seismic waves cannot constrain the time at which the 80 km discontinuity beneath OJP formed. One possibility is that it already existed, a compositional boundary related to depletion and dehydration that occurred at the ridge at the time the plate was formed. Discontinuities in this depth range are often imaged in the ocean basins (Gaherty et al., 1999; Rychert and Shearer, 2011; Tan and Helmberger, 2007). In this scenario compositional boundaries would need to persist despite the influence of plume melting, which might be challenging geodynamically.

Another possibility is that the ~282 km discontinuity may be related to a viscous root. How such a signature has persisted is not straightforward. For instance, a purely thermal anomaly would have dissipated within 50 My of the last volcanic pulse (Supplementary Fig. S1). Similarly, a purely thermal feature would not likely explain the sharp seismic velocity gradient observed at the base of the root or the low attenuation value for the region (Gomer and Okal, 2003). The anomalous velocity and discontinuity structure has persisted as the plateau traveled >8000 km WNW over the past 120 My since its formation. Such persistence would suggest considerable viscosity, which is consistent with the current tectonics of the region, where the rigid plateau is resisting subduction to the south, and SKS splitting suggests mantle flow is perturbed around the root (Klosko et al., 2001). Low attenuation values similarly support this interpretation (Gomer and Okal, 2003). Such a viscous root could be a result of volcanic formation ~120 My ago and/or the rejuvenation event ~90 My ago. This differs from the LAB interpretation of a velocity drop at 73 km depth beneath Hikurangi plateau (Stern et al., 2015). Hikurangi is thought to have formed in the same large melting event as OJP (Chandler et al., 2013). However, the deeper (>100 km) discontinuity structure of Hikurangi has yet to be investigated. In addition, the superplateau might have been laterally variable (Chandler et al., 2013) and the histories of the plateaus have diverged for 120 My.

One possible explanation for a viscous compositional root is that the magmatism and mantle upwelling that created the OJP may have left a lasting change on the residual mantle beneath, and large amounts of melting, >30%, could have removed the garnet from the peridotite, which would result in low seismic velocities in the root beneath 80 km (Schutt and Lesher, 2006). The melting would also likely deplete and dehydrate the residual mantle, producing a viscous root that extends to the depth of melting. A high temperature and wet plume could provide the deep solidus required beneath OJP. Alternatively, depleted compositions could be transported to deeper depths via complex convection patterns as demonstrated by laboratory experiments (Griffiths and Campbell, 1990) and geodynamic modeling (King and Anderson, 1998). Or, shortening of the root may have pushed material to greater depths during interaction with the subduction zone. This mechanism can easily be reconciled with low attenuation values in the region since bulk composition is not expected to affect seismic attenuation. However, this effect can only explain a 1% velocity anomaly (Schutt and Lesher, 2006), whereas our contrast at 80 km depth is 6%, and the region is 4–5% slow in comparison to surrounding regions (French et al., 2013; Richardson et al., 2000).

Velocity drops of greater magnitude could arise from subtle seismic anisotropy in concert with a compositional change, frozen melts, and/or more exotic mineralogies. Since SS is sensitive to impedance, density effects could also play a role. Melt may have percolated through deeper mantle, freezing above the 80 km discontinuity. A garnet-rich rock like eclogite could increase the density and velocity of the upper 80 km. Alternatively, garnet-rich amphibolite solidified from hydrous plume melts could be seismically fast, with the added attraction of a stability boundary at a similar depth range (Allen and Boettcher, 1983). Another possibility is that small amounts of wet partial melting aided the formation of seismically slow phlogopite (Wolbern et al., 2012) at >80 km depth. Observations of mantle peridotite from ophiolites and abyssal peridotites do not necessarily support large phlogopite percentages. However, another advantage of phlogopite is that it could 'dry-out' the olivine beneath 80 km, creating a relatively viscous mantle. Xenolith data from OJP support the notion of frozen melts and hydrous phases. There are abundant garnet-bearing pyroxenites <80 km depth and >100 km, with no garnet bearing xenoliths in between (Tommasi and Ishikawa, 2014). Additionally, there is evidence for metasomatism and the formation of amphibole, although it is much less abundant than the pyroxenite (Tommasi and Ishikawa, 2014). Similar metasomatic amphibole-rich layering has also been hypothesized to explain MLDs beneath the continents (Selway et al., 2015)

If a viscous root does exist to great depth beneath OJP, then the 80 km discontinuity is reminiscent of mid-lithospheric discontinuities (MLDs) observed beneath continental interiors, where xenoliths and seismic velocity anomalies support the existence of viscous roots to 200–250 km depth (Nettles and Dziewonski, 2008). One possibility is that large melting episodes in the Archean, similar to that which formed OJP, may have formed mid-lithospheric discontinuities observed within continental cratons today. This process may have been important in the early Archean for creating the continents, if subduction did not initiate until 3 Ga (Shirey and Richardson, 2011). Archean conditions and processes may have been much different from those operating today on OJP, i.e. higher mantle potential temperatures and possibly a stagnant lid. These higher temperatures likely enabled formation of thick basaltic crust, allowing formation of tonalite–tronghjemite–granodiorite (TTG) via remelting of eclogite from the base of the crust (Bedard, 2006). Indeed, no TTG suites typical of Archean continental crust have been found at OJP, probably because the crust beneath OJP may not have thickened enough to produce eclogite. However, regardless of the potential temperature, Archean and modern day plumes could both potentially impart frozen-in compositional boundaries.

5. Conclusions

We used SS precursors to image seismic discontinuity structure beneath northern OJP. Our inversions constrain a positive Moho discontinuity at 28 ± 4 km depth and deeper negative discontinu-

ities consistent with velocity decreases with depth at 80 ± 5 km and 282 ± 7 km. The result implies a thickened crust exists over a large lateral area of the northern plateau. The discontinuity at 282 km is not observed in our other ocean stacks, suggesting that the region may be anomalous to these depths. Thermal anomalies from the formation of the plateau via plume melting would have dissipated by now. Therefore, the persistence of anomalous structure at these depths in our result and those of others may suggest the existence of a viscous root, with the 282 km discontinuity potentially related to its base. The discontinuity at 80 km depth may be related to discontinuities observed across the Pacific at 60–110 km depth (Rychert and Shearer, 2011; Schmerr, 2012) and/or elastically accommodated grain boundary sliding. If it exists within a viscous root, the 80 km discontinuity is reminiscent of MLDs observed beneath continents. One possibility is that the 80 km discontinuity beneath OJP and possibly some MLD observations are compositional boundaries from previous large melting events.

Acknowledgements

We wish to thank Marc Hirschmann, for stimulating discussions. We thank the reviewers for their insightful comments that have significantly improved the discussion presented in this paper. The seismic dataset for the present study is available online at the Incorporated Research Institutions for Seismology (IRIS) Data Management Centre (DMC). This work is supported in part by NERC grants NE/K000985/1 and NE/M00788X/1.

Appendix A. Supplementary material

Supplementary material related to this article can be found online at http://dx.doi.org/10.1016/j.epsl.2016.06.026.

References

Aizawa, Y., Barnhoorn, A., Faul, U.H., Fitz Gerald, J.D., Jackson, I., Kovacs, I., 2008. Seismic properties of anita bay dunite: an exploratory study of the influence of water. J. Petrol. 49, 841–855. http://dx.doi.org/10.1093/petrology/egn007.

Aki, K., Richards, P.G., 2009. Quantative Seismology, second ed. University Science Books, California, ISBN 978-1-891389-63-4.

Allen, J.C., Boettcher, A.L., 1983. The stability of amphibole in andesite and basalt at high-pressures. Am. Mineral. 68, 307–314.

Bagley, B., Revenaugh, J., 2008. Upper mantle seismic shear discontinuities of the Pacific. J. Geophys. Res. 113. http://dx.doi.org/10.1029/2008jb005692.

Bedard, J.H., 2006. A catalytic delamination-driven model for coupled genesis of Archaean crust and sub-continental lithospheric mantle. Geochim. Cosmochim. Acta 70, 1188–1214. http://dx.doi.org/10.1016/j.gca.2005.11.008.

Beghein, C., Yuan, K.Q., Schmerr, N., Xing, Z., 2014. Changes in seismic anisotropy shed light on the nature of the Gutenberg discontinuity. Science 343, 1237–1240. http://dx.doi.org/10.1126/science.1246724.

Bostock, M.G., 1999. Seismic imaging of lithospheric discontinuities and continental evolution. Lithos 48, 1–16. http://dx.doi.org/10.1016/S0024-4937(99)00020-1.

Boyd, F.R., 1989. Compositional distinction between oceanic and cratonic lithosphere. Earth Planet. Sci. Lett. 96, 15–26. http://dx.doi.org/10.1016/0012-821x(89)90120-9.

Calvert, A.J., Sawyer, E.W., Davis, W.J., Ludden, J.N., 1995. Archean subduction inferred from seismic images of a mantle suture in the superior province. Nature 375, 670–674. http://dx.doi.org/10.1038/375670a0.

Chandler, M.T., Wessel, P., Sager, W.W., 2013. Analysis of Ontong Java Plateau palaeolatitudes: evidence for large-scale rotation since 123 Ma? Geophys. J. Int. 194, 18–29. http://dx.doi.org/10.1093/gji/ggt075.

Coffin, M.F., Eldholm, O., 1994. Large igneous provinces – crustal structure, dimensions, and external consequences. Rev. Geophys. 32, 1–36. http://dx.doi.org/10.1029/93rg02508.

Conder, J.A., Forsyth, D.W., Parmentier, E.M., 2002. Asthenospheric flow and asymmetry of the East Pacific Rise, MELT area. J. Geophys. Res. 107. http://dx.doi.org/10.1029/2001jb000807.

Cooper, P.A., Taylor, B., 1985. Polarity reversal in the Solomon-islands Arc. Nature 314, 428–430. http://dx.doi.org/10.1038/314428a0.

Covellone, B.M., Savage, B., Shen, Y., 2015. Seismic wave speed structure of the Ontong Java Plateau. Earth Planet. Sci. Lett. 420, 140–150. http://dx.doi.org/10.1016/j.epsl.2015.03.033.

Deuss, A., Woodhouse, J.H., 2002. A systematic search for mantle discontinuities using SS-precursors. Geophys. Res. Lett. 29. http://dx.doi.org/10.1029/2002gl014768.

Dziewonski, A.M., Anderson, D.L., 1981. Preliminary reference Earth model. Phys. Earth Planet. Inter. 25, 297–356. http://dx.doi.org/10.1016/0031-9201(81)90046-7.

Faul, U.H., 1997. Permeability of partially molten upper mantle rocks from experiments and percolation theory. J. Geophys. Res. 102, 10299–10311. http://dx.doi.org/10.1029/96jb03460.

French, S., Lekic, V., Romanowicz, B., 2013. Waveform tomography reveals channeled flow at the base of the oceanic asthenosphere. Science 342, 227–230. http://dx.doi.org/10.1126/Science.1241514.

Fukao, Y., Obayashi, M., 2013. Subducted slabs stagnant above, penetrating through, and trapped below the 660 km discontinuity. J. Geophys. Res. 118, 5920–5938. http://dx.doi.org/10.1002/2013jb010466.

Furumoto, A.S., Webb, J.P., Odegard, M.E., Hussong, D.M., 1976. Seismic studies on the Ontong Java Plateau, 1970. Tectonophysics 34, 71–90. http://dx.doi.org/10.1016/0040-1951(76)90177-3.

Gaherty, J.B., Kato, M., Jordan, T.H., 1999. Seismological structure of the upper mantle: a regional comparison of seismic layering. Phys. Earth Planet. Inter. 110, 21–41. http://dx.doi.org/10.1016/S0031-9201(98)00132-0.

Gladczenko, T.P., Coffin, M.F., Eldholm, O., 1997. Crustal structure of the Ontong Java Plateau: modeling of new gravity and existing seismic data. J. Geophys. Res. 102, 22711–22729. http://dx.doi.org/10.1029/97jb01636.

Gomer, B.M., Okal, E.A., 2003. Multiple-ScS probing of the Ontong-Java Plateau. Phys. Earth Planet. Inter. 138, 317–331. http://dx.doi.org/10.1016/S0031-9201(03)00114-6.

Griffiths, R.W., Campbell, I.H., 1990. Stirring and structure in mantle starting plumes. Earth Planet. Sci. Lett. 99, 66–78. http://dx.doi.org/10.1016/0012-821x(90)90071-5.

Harmon, N., Blackman, D.K., 2010. Effects of plate boundary geometry and kinematics on mantle melting beneath the back-arc spreading centers along the Lau Basin. Earth Planet. Sci. Lett. 298, 334–346. http://dx.doi.org/10.1016/j.epsl.2010.08.004.

Hayes, G.P., Wald, D.J., Johnson, R.L., 2012. Slab1.0: a three-dimensional model of global subduction zone geometries. J. Geophys. Res. 117. http://dx.doi.org/10.1029/2011jb008524.

Hirschmann, M.M., 2010. Partial melt in the oceanic low velocity zone. Phys. Earth Planet. Inter. 179, 60–71. http://dx.doi.org/10.1016/J.Pepi.2009.12.003.

Hirth, G., Kohlstedt, D.L., 1995. Experimental constraints on the dynamics of the partially molten upper-mantle – deformation in the diffusion creep regime. J. Geophys. Res. 100, 1981–2001. http://dx.doi.org/10.1029/94jb02128.

Hirth, G., Kohlstedt, D.L., 1996. Water in the oceanic upper mantle: implications for rheology, melt extraction and the evolution of the lithosphere. Earth Planet. Sci. Lett. 144, 93–108. http://dx.doi.org/10.1016/0012-821x(96)00154-9.

Ito, G., Clift, P.D., 1998. Subsidence and growth of Pacific Cretaceous plateaus. Earth Planet. Sci. Lett. 161, 85–100. http://dx.doi.org/10.1016/S0012-821x(98)00139-3.

Ito, G., Taira, A., 2000. Compensation of the Ontong Java Plateau by surface and subsurface loading. J. Geophys. Res. 105, 11171–11183. http://dx.doi.org/10.1029/2000jb900036.

Jackson, I., Faul, U.H., 2010. Grainsize-sensitive viscoelastic relaxation in olivine: towards a robust laboratory-based model for seismological application. Phys. Earth Planet. Inter. 183, 151–163. http://dx.doi.org/10.1016/J.Pepi.2010.09.005.

Jha, K., Parmentier, E.M., Morgan, J.P., 1994. The role of mantle-depletion and melt-retention buoyancy in spreading-center segmentation. Earth Planet. Sci. Lett. 125, 221–234. http://dx.doi.org/10.1016/0012-821x(94)90217-8.

Karato, S., Wu, P., 1993. Rheology of the upper mantle – a synthesis. Science 260, 771–778. http://dx.doi.org/10.1126/science.260.5109.771.

Karato, S.I., Olugboji, T., Park, J., 2015. Mechanisms and geologic significance of the mid-lithosphere discontinuity in the continents. Nat. Geosci. 8, 509–514. http://dx.doi.org/10.1038/Ngeo2462.

Katz, R.F., Spiegelman, M., Langmuir, C.H., 2003. A new parameterization of hydrous mantle melting. Geochem. Geophys. Geosyst. 4. http://dx.doi.org/10.1029/2002gc000433.

Kawakatsu, H., Kumar, P., Takei, Y., Shinohara, M., Kanazawa, T., Araki, E., Suyehiro, K., 2009. Seismic evidence for sharp lithosphere–asthenosphere boundaries of oceanic plates. Science 324, 499–502. http://dx.doi.org/10.1126/science.1169499.

King, S.D., Anderson, D.L., 1998. Edge-driven convection. Earth Planet. Sci. Lett. 160, 289–296. http://dx.doi.org/10.1016/S0012-821x(98)00089-2.

Klosko, E.R., Russo, R.M., Okal, E.A., Richardson, W.P., 2001. Evidence for a rheologically strong chemical mantle root beneath the Ontong-Java Plateau. Earth Planet. Sci. Lett. 186, 347–361. http://dx.doi.org/10.1016/S0012-821x(01)00235-7.

Korenaga, T., Korenaga, J., 2008. Subsidence of normal oceanic lithosphere, apparent thermal expansivity, and seafloor flattening. Earth Planet. Sci. Lett. 268, 41–51. http://dx.doi.org/10.1016/j.epsl.2007.12.022.

Lee, C.T.A., Luffi, P., Chin, E.J., 2011. Building and destroying continental mantle. Annu. Rev. Earth Planet. Sci. 39, 59–90. http://dx.doi.org/10.1146/annurev-earth-040610-133505.

Maggi, A., Debayle, E., Priestley, K., Barruol, G., 2006. Azimuthal anisotropy of the Pacific region. Earth Planet. Sci. Lett. 250, 53–71. http://dx.doi.org/10.1016/J.Epsl.2006.07.010.

Mann, P., Taira, A., 2004. Global tectonic significance of the Solomon Islands and Ontong Java Plateau convergent zone. Tectonophysics 389, 137–190. http://dx.doi.org/10.1016/j.tecto.2003.10.024.

Miura, S., Suyehiro, K., Shinohara, M., Takahashi, N., Araki, E., Taira, A., 2004. Seismological structure and implications of collision between the Ontong Java Plateau and Solomon Island Arc from ocean bottom seismometer – airgun data. Tectonophysics 389, 191–220. http://dx.doi.org/10.1016/j.tecto.2003.09.029.

Muller, R.D., Dutkiewicz, A., Seton, M., Gaina, C., 2013. Seawater chemistry driven by supercontinent assembly, breakup, and dispersal. Geology 41, 907–910. http://dx.doi.org/10.1130/G34405.1.

Nettles, M., Dziewonski, A.M., 2008. Radially anisotropic shear velocity structure of the upper mantle globally and beneath North America. J. Geophys. Res. 113. http://dx.doi.org/10.1029/2006jb004819.

Richardson, W.P., Okal, E.A., Van der Lee, S., 2000. Rayleigh-wave tomography of the Ontong-Java Plateau. Phys. Earth Planet. Inter. 118, 29–51. http://dx.doi.org/10.1016/S0031-9201(99)00122-3.

Rychert, C.A., Fischer, K.M., Rondenay, S., 2005. A sharp lithosphere–asthenosphere boundary imaged beneath eastern North America. Nature 436, 542–545. http://dx.doi.org/10.1038/Nature03904.

Rychert, C.A., Harmon, N., Schmerr, N., 2014. Synthetic waveform modelling of SS precursors from anisotropic upper-mantle discontinuities. Geophys. J. Int. 196, 1694–1705. http://dx.doi.org/10.1093/gji/ggt474.

Rychert, C.A., Shearer, P.M., 2009. A global view of the lithosphere–asthenosphere boundary. Science 324, 495–498. http://dx.doi.org/10.1126/science.1169754.

Rychert, C.A., Shearer, P.M., 2010. Resolving crustal thickness using SS waveform stacks. Geophys. J. Int. 180, 1128–1137. http://dx.doi.org/10.1111/j.1365-246X.2009.04497.x.

Rychert, C.A., Shearer, P.M., 2011. Imaging the lithosphere–asthenosphere boundary beneath the Pacific using SS waveform modeling. J. Geophys. Res. 116. http://dx.doi.org/10.1029/2010jb008070.

Rychert, C.A., Shearer, P.M., Fischer, K.M., 2010. Scattered wave imaging of the lithosphere–asthenosphere boundary. Lithos 120, 173–185. http://dx.doi.org/10.1016/j.lithos.2009.12.006.

Schmerr, N., 2012. The Gutenberg discontinuity: melt at the lithosphere–asthenosphere boundary. Science 335, 1480–1483. http://dx.doi.org/10.1126/science.1215433.

Schutt, D.L., Lesher, C.E., 2006. Effects of melt depletion on the density and seismic velocity of garnet and spinel lherzolite. J. Geophys. Res. 111. http://dx.doi.org/10.1029/2003jb002950.

Selway, K., Ford, H., Kelemen, P., 2015. The seismic mid-lithosphere discontinuity. Earth Planet. Sci. Lett. 414, 45–57. http://dx.doi.org/10.1016/j.epsl.2014.12.029.

Shirey, S.B., Richardson, S.H., 2011. Start of the Wilson cycle at 3 Ga shown by diamonds from subcontinental mantle. Science 333, 434–436. http://dx.doi.org/10.1126/Science.1206275.

Smolarkiewicz, P.K., 1984. A fully multidimensional positive definite advection transport algorithm with small implicit diffusion. J. Comput. Phys. 54, 325–362. http://dx.doi.org/10.1016/0021-9991(84)90121-9.

Stern, T.A., Henrys, S.A., Okaya, D., Louie, J.N., Savage, M.K., Lamb, S., Sato, H., Sutherland, R., Iwasaki, T., 2015. A seismic reflection image for the base of a tectonic plate. Nature 518, 85–88. http://dx.doi.org/10.1038/nature14146.

Tan, Y., Helmberger, D.V., 2007. Trans-Pacific upper mantle shear velocity structure. J. Geophys. Res. 112. http://dx.doi.org/10.1029/2006jb004853.

Taylor, S.R., Mclennan, S.M., 1995. The geochemical evolution of the continental-crust. Rev. Geophys. 33, 241–265. http://dx.doi.org/10.1029/95RG00262.

Tommasi, A., Ishikawa, A., 2014. Microstructures, composition, and seismic properties of the Ontong Java Plateau mantle root. Geochem. Geophys. Geosyst. 15, 4547–4569. http://dx.doi.org/10.1002/2014gc005452.

Wolbern, I., Rumpker, G., Link, K., Sodoudi, F., 2012. Melt infiltration of the lower lithosphere beneath the Tanzania craton and the Albertine rift inferred from S receiver functions. Geochem. Geophys. Geosyst. 13. http://dx.doi.org/10.1029/2012gc004167.